Microchimica Acta (2022) 189: 248
https://doi.org/10.1007/s00604-022-05350-1

ORIGINAL PAPER

Dual-readout immunosensor based on multifunctional MXene probe triggers the signal amplification for detection of autoimmune hepatitis marker

Sha Liu[1] · Xiaofeng Li[2] · Yanjie Chen[1] · Yitian Huang[1] · Shupei Zhang[3] · Hong Dai[1]

Received: 7 March 2022 / Accepted: 16 May 2022 / Published online: 9 June 2022

Abstract

A dual-readout immunosensor coupled with electrochemical impedance and temperature signal was successfully proposed to detect autoimmune hepatitis markers (ASGPR). Nb_2C MXene with excellent conductivity, abundant surface functional groups, and extraordinary photothermal conversion efficiency, was designed to be a multifunctional biological probe, whose specific binding with antigen enhanced steric hindrance to generate electrochemical impedance signal, and at the same time, it had a strong optical response in the near-infrared band to achieve temperature output. In addition, poly(N-isopropyl acrylamide) (PNIPAM) was a temperature-sensitive polymer, which was adopted as the sensing matrix. When the multifunctional probe was specifically bound to the antigen, under 808-nm laser irradiation, the captured Nb_2C MXene achieved photothermal conversion to increase the electrode surface temperature, and the conformation of PNIPAM changed from a free spiral to a spherical shape, further realizing double amplification of the EIS signal. Under the optimized experimental conditions, the impedance values and the temperature changes increased proportionally with the increase of the ASGPR concentration from 10^{-5} to 1 ng/mL, and the detection limit of the immunosensor was 3.3×10^{-6} ng/mL. The established dual-readout immunosensor exhibited good selectivity and acceptable stability and provided an effective detection method for autoimmune hepatitis marker detection.

Keywords Dual-readout · Impedimetric immunosensor · Signal amplification · PNIPAM · Nb_2C MXene · ASGPR

Introduction

In 2010, the World Health Organization investigated foodborne cases, of which nearly 30,000 people died of hepatitis A [1]. Hepatitis A is an acute liver infection that increases in severity with age [2] and is ultimately life-threatening [3]. Therefore, it is of great significance to find a biomarker for the early diagnosis of hepatitis A and improve the survival rate of patients. Asialoglycoprotein receptor (ASGPR) is a transmembrane protein located on the surface of hepatocytes. Studies have shown that ASGPR is a liver-specific target antigen [4, 5]. Therefore, ASGPR can be used as a reliable biomarker for early diagnosis of hepatitis A.

Up to now, various analytical measures, such as fluorescence analysis [6], magnetic resonance imaging (MRI) [7], and inductively coupled plasma mass spectrometry (ICP-MS) [8], have been applied in ASGPR detection. While long time-consuming, tedious sample preparation and complicated operations limit their wide application. Conversely, electrochemical immunoassay is an attractive analytical method, which has attracted wide attention in biological analysis because of its advantages of fast response, high sensitivity, and low cost. In particular, the electrochemical impedance spectroscopy (EIS) method could not only detect the interaction of biomolecules by measuring changes in impedance but also measure the response of the electrochemical system to the applied oscillation potential as a function of frequency [9], which has good anti-interference

Sha Liu and Xiaofeng Li contributed to the work equally and should be regarded as co-first author.

✉ Hong Dai
dhong@fjnu.edu.cn

1 College of Chemistry and Material, Fujian Normal University, Fuzhou 350108, Fujian, China

2 Department of Neurology, Union Hospital, Fuzhou 350002, Fujian, China

3 College of Chemical and Material Engineering, Quzhou University, Quzhou 32400, Zhejiang, China

ability. However, most impedance immunosensors are in a single readout mode, which is easily affected by external interference and systematic errors, leading to false-positive or false-negative results. To address these issues and improve the accuracy of detection results, dual-readout immunosensors that output two signals simultaneously are urgently needed [10]. Until now, the dual-readout immunosensor coupled with EIS and PEC (photoelectrochemical) has been studied for detecting tumor markers [11]. Unfortunately, it inevitably used complex instruments and professional personnel. Therefore, looking for an electrochemical impedance immunosensor combined with a simple signal reading will help to expand its application range. In order to achieve this goal, this work first proposed a dual-readout immunosensor based on electrochemical impedance spectroscopy and temperature signal to detect ASGPR.

To develop an ultrasensitive EIS immunoassay method with higher specificity and lower detection limit, a signal amplification strategy has been used to amplify the response signal to detect classic biomarkers. Amplifying the measurable signal and reducing the background were two important ways to improve the sensitivity of EIS immunosensors. For example, many studies have used nanomaterials to modify substrates to increase the immobilization of antibodies on the electrode surface, improving the background capacity and signal-to-noise ratio of immunosensors [12]. In addition, the introduction of conducting polymers into immunosensors improved the conductivity of the device, opening up signal amplification for EIS immunosensors [13]. However, the electrical conductivity of polymers was tied to the degree of protonation, often requiring specific acidic environments. At the same time, these amplification methods required additional molecular recognition elements and expensive signaling tags, limiting their application in biotechnology. Therefore, it was still urgent to develop simple and cost-effective amplification proposals. It has been reported that increasing the electrode surface temperature can accelerate the reaction kinetics of electroactive substances and enhance the electrochemical signal [14]. Therefore, it was a great challenge to find an efficient method to increase the electrode surface temperature.

So far, microheaters [15] and electrical heating techniques [16] have been applied to increase the electrode surface temperature. Herein, a novel Nb_2C MXene photothermal material was cleverly introduced [17], which was a carbide composed of two-dimensional metal carbides and transition metals [18, 19]. Due to its abundant surface functional groups and excellent photothermal conversion ability [20–22], Nb_2C MXene was designed as a multifunctional probe, under 808-nm laser irradiation, as thermal conversion devices to realize the photothermal conversion process, efficiently convert light into heat, and generate high temperature in the local area of the electrode surface, which greatly shortens the reaction time. Furthermore, the type of electrode material and the modification method of the electrode surface would affect the performance of EIS immunosensors [23, 24]. Among them, the modification of the sensing interface played an irreplaceable role in ultrasensitive EIS immunosensors. Hou's group reported that the electrodeposition of gold nanoparticles was used to modify the glassy carbon electrode interface; insoluble precipitates were generated by enzyme-mediated biocatalytic precipitation reactions, thereby amplifying the EIS signal [25]. Considering that the phase transition behavior of polymers under 808-nm laser irradiation was a tool to effectively tune the sensing interface, for this purpose, our work was motivated by combining a near-infrared (NIR) responsive polymer with Nb_2C MXene materials to build a temperature-EIS coupled sensing platform. In this case, stimuli-responsive polymers could serve as a bridge between EIS and biomarker detection. PNIPAM was a stimulus-responsive polymer, when external conditions such as light or temperature change, it can significantly change the electrochemical behavior of the interface [26]. The temperature is used as a trigger; Nb_2C MXene and PNIPAM have a synergistic effect to complete the expansion-collapse transition. When there is no laser irradiation, the electrode surface temperature is lower than LCST (low critical solution temperature); due to the hydrogen bond between the amide group of PNIPAM and water molecules, the water molecules are arranged around PNIPAM in an orderly manner, making PNIPAM dissolves in water in the form of random coils, and PNIPAM is in "expansion" state. On the contrary, after the photothermal probe specifically binds to the antigen, the surface temperature of the electrode rises through photothermal conversion by 808-nm laser irradiation, when $T > LCST$, the molecular thermal motion is intensified, the hydrophobic interaction between isopropyl groups is enhanced, and a hydrophobic layer is formed. The PNIPAM chain collapses into a spherical shape and is in a "contracted" state. After 808-nm laser irradiation, they show a volume-phase change from an expanded state to a collapsed state, which further realized the Nb_2C MXene multifunctional probe photothermal trigger signal amplification process.

In this work, an EIS and temperature dual-readout immunosensor were constructed for the sensitive determination of ASGPR by utilizing a multifunctional probe of Nb_2C MXene. As shown in Scheme 1, the PNIPAM with unique temperature sensitivity was used as an immunosensor platform, which provided a large number of immobilization sites for primary antibody (Ab_1). The Nb_2C MXene labeled secondary antibody (Ab_2) as a multifunctional biological probe (Nb_2C MXene@Ab_2), realizing the sensitive detection of ASGPR by the sandwich-type protocol. Among them, the

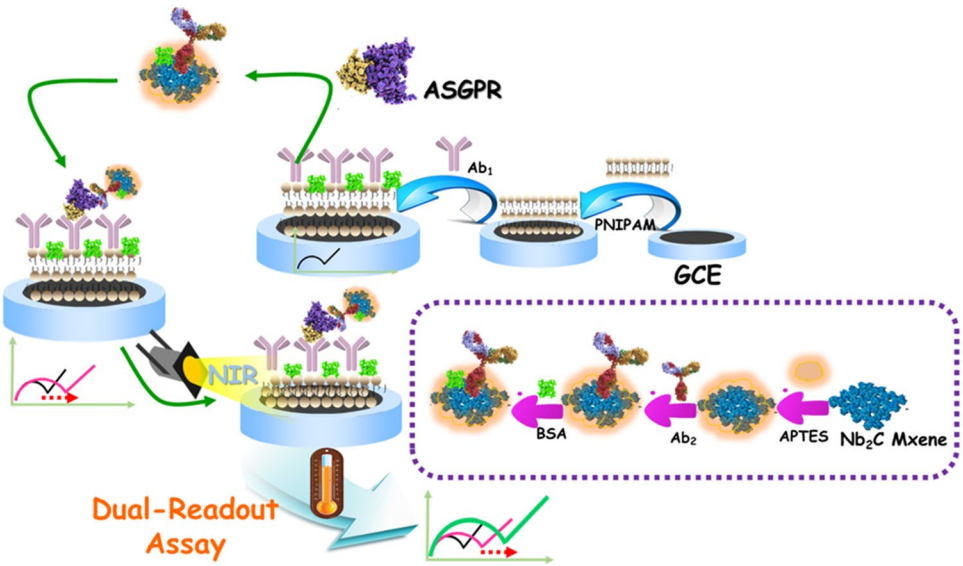

Scheme 1 Schematic illustration of the dual-mode immunoassay for autoimmune hepatitis marker

Nb_2C MXene multifunctional probe could not only produce electrochemical impedance signal output by immunoreaction with antigen, but also as a thermal conversion unit to achieve temperature signal output. When the Nb_2C MXene@Ab_2 was immunized with the antigen, under 808-nm laser irradiation, PNIPAM has undergone a conformational change, which further realized the double amplification of the EIS signal. This study expanded the application of Nb_2C MXene in dual-readout immunosensors and also provides new ideas for exploring other biomarkers.

Experimental section

Materials and reagents

N-Isopropylacrylamide (NIPAm) was purchased from Huateng Pharmaceutical Co., Ltd. Both ammonium persulfate (APS) and N,N′-methylenebisacrylamide (BIS) were purchased by Sinopharm Chemical Reagent Co., Ltd. (Shanghai, China). Glutaraldehyde (GLD), N,N,N′,N′-tetramethylethylenediamine (TEMED), and (3-aminopropyl)triethoxysilane (APTES) were purchased from Aladdin Chemical Co., Ltd. (Shanghai, China). Lipolysis-stimulated lipoprotein receptor (LSR) and Interleukin-6 (IL-6) were purchased from Linc-Bio Science Co., Ltd. (Shanghai, China). ASGPR standard solution, its primary antibody (Ab1), and secondary antibody (Ab2) were purchased from Chundu Biotechnology Co., Ltd. (Wuhan, China). Sheep serum albumin (BSA) was purchased from Bioss Biology Technology (Beijing, China). Human serum samples from healthy donors were provided by Fujian Provincial Maternity and Child Health Hospital. Phosphate-buffered saline (PBS) was prepared by adjusting the pH. Deionized water was used throughout the experiment.

Apparatus

Electrochemical impedance spectroscopy (EIS) and cyclic voltammetry experiments were measured with a CHI760 electrochemical workstation (Shanghai Chenhua Instrument Co., Ltd., Shanghai, China). The materials were further characterized by transmission electron microscope (TEM, FEI F20 S-TWIN instrument) and scanning electron microscope (SEM, SU8000 instrument). A digital thermometer (TES Electric and Electronics Co., Taiwan, China) was used to measure temperature. The experiment used a three-electrode system, which consisted of a modified glass carbon electrode (GCE) as the working electrode, Ag/AgCl as the reference electrode, and platinum wire as the auxiliary electrode.

Synthesis of PNIPAM

PNIPAM were synthetized according to the previous report [27]. Firstly, 0.1377 g of n-isopropylacrylamide (NIPAm), 0.05 N,N′-methylenebisacrylamide (BIS), and 0.0116 mercaptoethylamine were added to 5 mL of water and stirred to make the dispersion uniform. Subsequently, filled with nitrogen for 20 min to remove oxygen and quickly added the accelerator N,N,N′,N′-tetramethylethylenediamine (TEMED). Finally, the initiator ammonium persulfate (APS) was added to further initiate the reaction to complete, and the PNIPAM polymer was synthesized by standing at room temperature.

Synthesisof Nb_2C MXene

The preparation process of Nb_2C was according to the previous report with small modification [28]. Detailed material synthesis was shown in Supporting Information 1.

Synthesis ofmultifunctional Nb_2C MXeneprobe

Firstly, 200 µL of 5 mg/mL Nb_2C and 100 µL of 1wt% (3-aminopropyl) triethoxysilane (APTES) were mixed for functionalization at room temperature for 6 h and washed with deionized water by centrifugation three times. Subsequently, 200 µL 2.5 wt% of glutaraldehyde (GLD) was added to the shaker to absorb for 50 min, and it was covalently coupled with the added secondary antibody (Ab_2), and 1 wt% BSA was used to block non-specific sites and finally washed with deionized water. The obtained Nb_2C MXene-APTES-Ab_2 (Ab_2 bioconjugate) was finally stored at a temperature of 4 °C for use.

Construction of immunosensor

Initially, the bare GCE was polished with 0.03-µm alumina powder and rinsed with deionized water. The electrode was modified with 5 µL PNIPAM and dried at room temperature, 5 µL GLD (2.5 wt%), and 5 µL Ab_1 (10 ng/mL) were dropped on the electrode surface and incubated at 4 °C for 50 min. To prevent the adsorption of non-specific sites, 5 µL BSA (1 wt%) was added to the electrode surface for blocking. Subsequently, 5 µL of ASGPR standard solutions of different concentrations were added to the electrode and incubated for 30 min at 4 °C to obtain ASGPR/Ab_1/PNIPAM/GCE. Finally, the obtained electrode and Ab_2 bioconjugate were incubated for 50 min at 4 °C to complete the immunosensing structure. After each step of modification, they were gently dipped and washed with deionized water.

Result and discussion

Characterizations of materials

Transmission electron microscopy (TEM) and scanning electron microscopy (SEM) were used to characterize the structure and morphology of Nb_2C MXene. Figure 1A showed a TEM image of a few-layer or single-layer Nb_2C MXene. The transparent flake shape could be clearly observed, which showed that the Nb_2C has only a few layers in several atomic layers. Figure 1B showed a SEM image of Nb_2C MXene; the aluminum atomic layer was successfully removed by HF during etching, forming a unique accordion-like multilayer Nb_2C MXene structure. As shown in Fig. 1C, Fourier transform infrared spectroscopy (FT-IR) was used to study the difference of functional groups before and after the functionalization of Nb_2C MXene. Nb_2C MXene FT-IR spectrum showed (curve a); the sharp peaks at 3442 cm^{-1} and 1602 cm^{-1} were hydrogen-bonded hydroxyl groups, which proved the high hydrophilicity of Nb_2C MXene. In addition, the peak at 2890 cm^{-1} was the C-H tensile vibration [29]. The functionalized Nb_2C-APTES (curve b) FT-IR spectrum showed that there were additional peaks in the Nb_2C-APTES spectrum, and there was Si–O stretching vibration at the position of 1100 cm^{-1}, indicating that the success of the amino-terminal silane ground was connected to the surface of Nb_2C MXene. There was C-NH_2 tensile vibration at the position of 1552 cm^{-1}, further indicating that Nb_2C MXene was successfully functionalized by APTES [30].

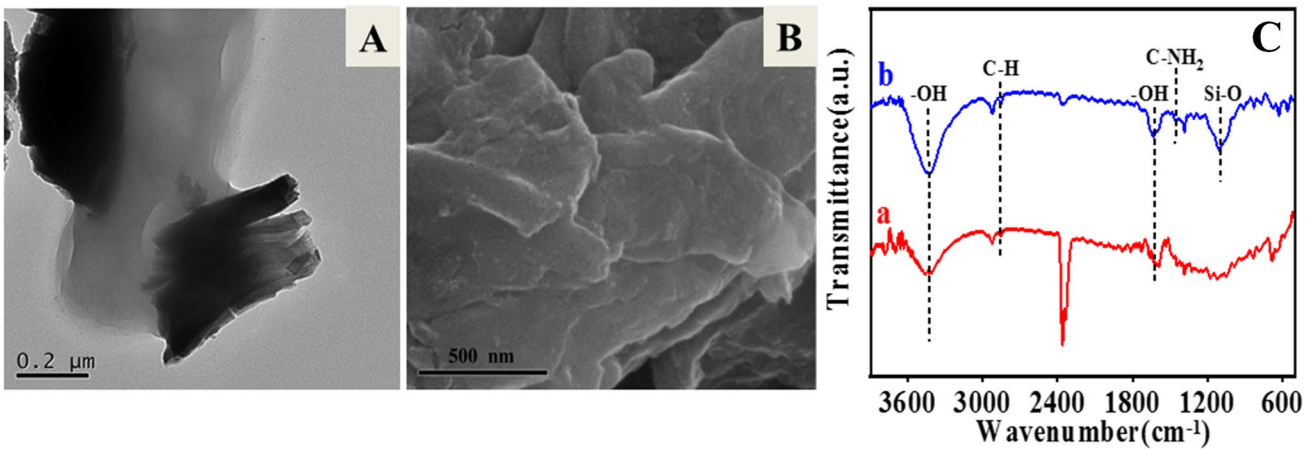

Fig. 1 The TEM image of **A** Nb_2C MXene, **B** the SEM image of MXene, and **C** the FT-IR spectrum (a) Nb_2C MXene, (b) functionalized Nb_2C-APTES

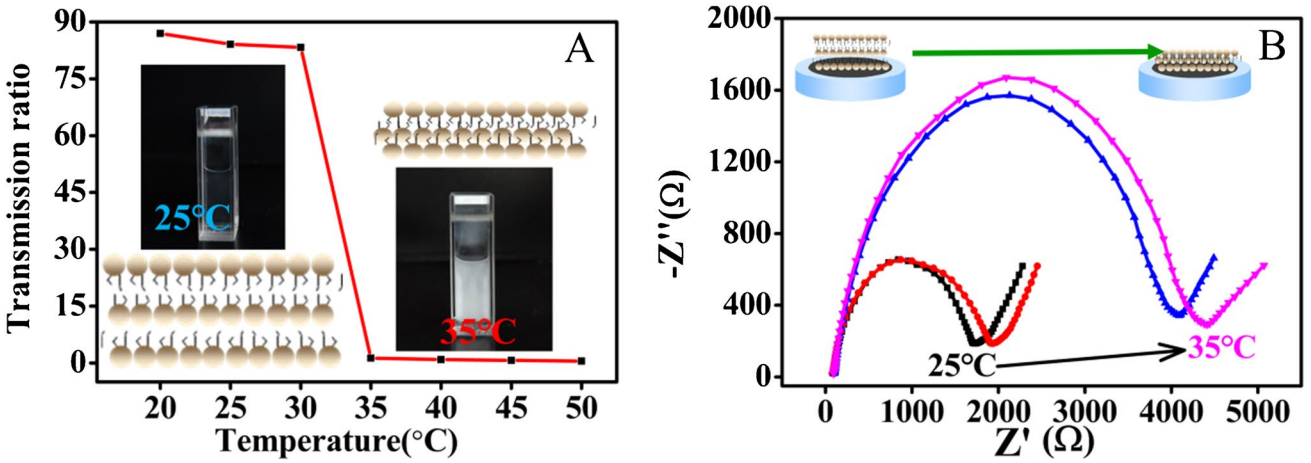

Fig. 2 **A** The transmittance of poly(N-isopropylacrylamide) PNIPAM at different temperatures. Insert: the shrinkage behavior of pNIPAM at different temperatures is 25 °C (top left) and 35 °C (bottom right). **B** Electrochemical impedance response of PNIPAM hydrogel at 25 °C, 28 °C, 32 °C, 35 °C in 0.1 M KCl containing 5.0 mM $[Fe(CN)6]^{3-}/^{4-}$

Shrinkage behavior of thermosensitive PNIPAM

Fig. 2A showed the transmittance of the temperature-sensitive polymer PNIPAM at different temperatures. With the increase of temperature, the transmittance gradually decreased. It was worth noting that the transmittance decreased sharply at 30–35 °C, indicating that PNIPAM has undergone phase transition behavior in this temperature region. In addition, PNIPAM entered a shrinking state at 35 °C, and the appearance became opaque (inset of Fig. 2A). As depicted in Fig. 2B, when PNIPAM was covered on the electrode, the value of R_{ct} gradually increased with the increase of temperature, and the R_{ct} value increased significantly at 32 °C. This trend was attributed to the expansion of PNIPAM when the temperature was lower than 32 °C; when the temperature was higher than 32 °C, PNIPAM underwent hydrophobic shrinkage, which hindered the diffusion of ferricyanide to the electrode surface [31]

Photothermalperformance of multifunctional Nb_2C MXene

The Nb_2C MXene exhibited a wide absorption band in the near-infrared region, indicating that Nb_2C MXene had strong near-infrared laser absorption capability (Figure S1). Therefore, we have chosen to study the photothermal properties of the material by irradiating various concentrations of Nb_2C MXene with 808-nm laser light for 300 s (2.5 w/cm^2 of power density). As shown in Fig. 3A, under laser irradiation, the water temperature hardly changed. At the same time, the temperature of Nb_2C MXene gradually increased as the irradiation time increased, and eventually stabilized. Figure 3B showed that the temperature of Nb_2C MXene (5 mg/mL) increased with the increase of laser power. It has been proved that Nb_2C MXene has shown outstanding light-to-heat conversion performance due to its excellent electromagnetic wave absorption ability and localized surface plasmon resonance effect. Figure 3C studied the photothermal properties of different materials. The functionalized Nb_2C MXene had a faster temperature change than Nb_2C MXene, due to the lower binding energy of Nb_2C MXene-APTES. As shown in Fig. 3D, the photothermal stability of functionalized Nb_2C was studied, and the results showed that it had a relatively stable value within 5 irradiation cycles, indicating that Nb_2C MXene-APTES had excellent stability.

Fabrication of dual-readout immunosensor

CV and EIS were evaluation strategies to gradually modify the electrode interface. First, the manufacturing process of the immunosensor was studied by cyclic voltammetry (CV). As shown in Fig. 4A, a pair of oxidation and reduction peaks were observed (curve a). However, after the PNIPAM polymer was modified on GCE, due to the dense internal structure and film-forming characteristics of PNIPAM, the diffusion speed of redox substances to the electrode interface slowed down, and the peak current decreased (curve b). After Ab_1, ASGPR and the probe were fixed in sequence; they formed protein macromolecules with large steric hindrance, so the peak current gradually decreased (curve c–e). When an 808 nm (2.5 w/cm^2) laser was used to irradiate the electrode for 30 s, the PNIPAM polymer was shrinking status, and the peak current dropped sharply (curve f). The above results indicated that the immunosensor was

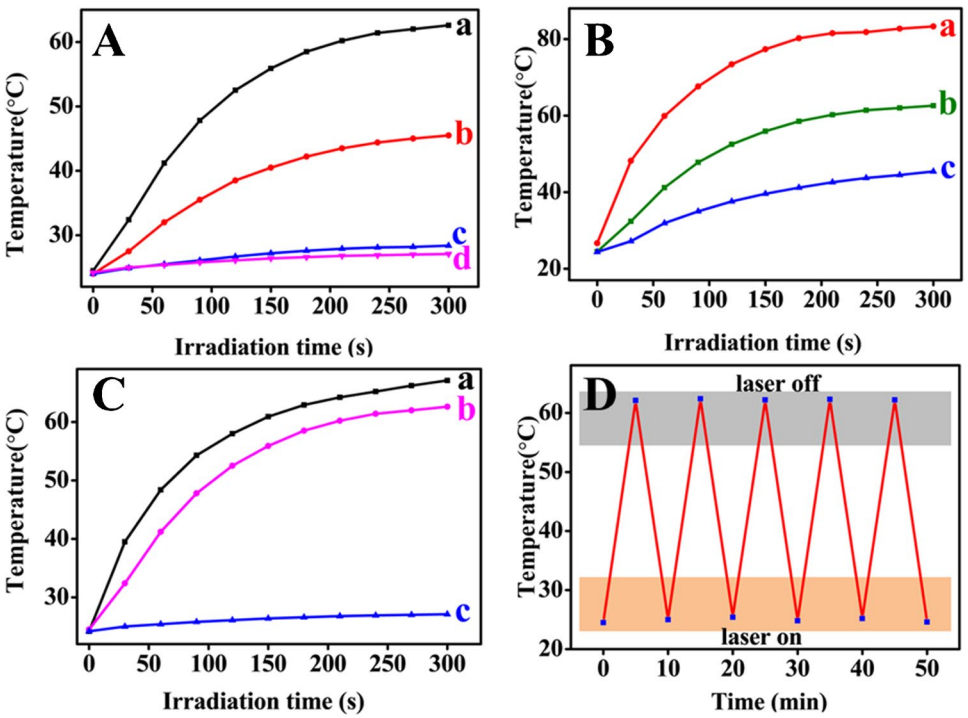

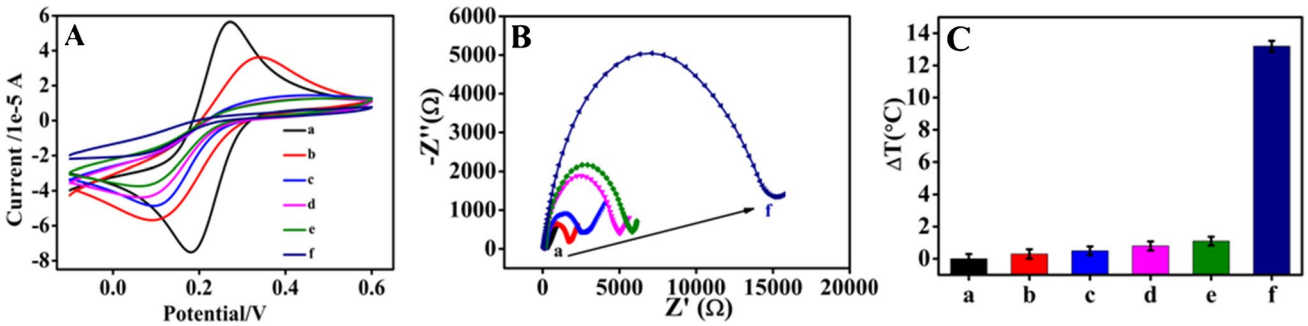

Fig. 3 **A** The photothermal effect of Nb_2C MXene (808 nm, 2.5 w/cm^{-2}) of (a) 5 mg/mL Nb_2C, (b) 1 mg/mL Nb_2C, (c) 0.1 mg/mL Nb_2C, (d), water. **B** The photothermal effect of Nb_2C MXene (5 mg/mL) under different laser power densities of (a) 3 w/cm^{-2}, (b) 2.5 w/cm^{-2}, (c) 2 w/cm.$^{-2}$. **C** The photothermal effect of different materials. (a) Nb_2C, (b) functionalized Nb_2C-APTES, (d) water. **D** Photothermal stability of functionalized Nb_2C MXene (5 mg/mL) upon 5 cycles of 808-nm laser on/off

Fig. 4 **A** CV, **B** EIS curves, and **C** temperature increase of different electrodes: (a) GCE, (b) PNIPAM/GCE, (c) Ab_1/PNIPAM/GCE, (d) ASGPR/Ab_1/PNIPAM/GCE, (e) Nb_2C-APTES-Ab_2/ASGPR/Ab_1/PNIPAM/GCE, (f) irradiate Nb_2C-APTES-Ab_2/ASGPR/Ab_1/PNIPAM/GCE with near-infrared light

successfully constructed. At the same time, the assembly process of the immunosensor was further studied through the R_{ct} and temperature changes of the electrode. As shown in Fig. 4B and Fig. 4C, the EIS signal gradually increased without laser irradiation, but the change was small, and the temperature change was also very small (curve a–e). Under laser irradiation, Nb_2C MXene converted light into heat, which increased the electrode surface temperature; the surface temperature of the electrode was higher than the LCST of PNIPAM, causing a conformational change. At this time, PNIPAM transformed from a free coil shape to a spherical body, tightly wrapped on the surface of the electrode, which hindered the charge transfer on the surface of the electrode; a strong EIS signal was generated and temperature increased to maximum (curve f). The above results were consistent with the CV results, indicating the successful construction of the dual-mode immunosensor.

Analytical performance of the immunoassay

In order to obtain the best analytical performance, the experimental conditions such as Ab_1, ASGPR, probe incubation time (Figure S2), irradiation time, and light intensity (Figure S3) were optimized. Under the best experimental conditions, the dual-readout immunoassay method was used to detect different concentrations of ASGPR. As shown in Fig. 5A, the impedance increased as the concentration of ASGPR increased (a–f). In addition, through the R_{ct} value and the ASGPR concentration logarithm from 10^{-5} to 1 ng/mL, a good linear relationship was obtained (insert Fig. 5B).

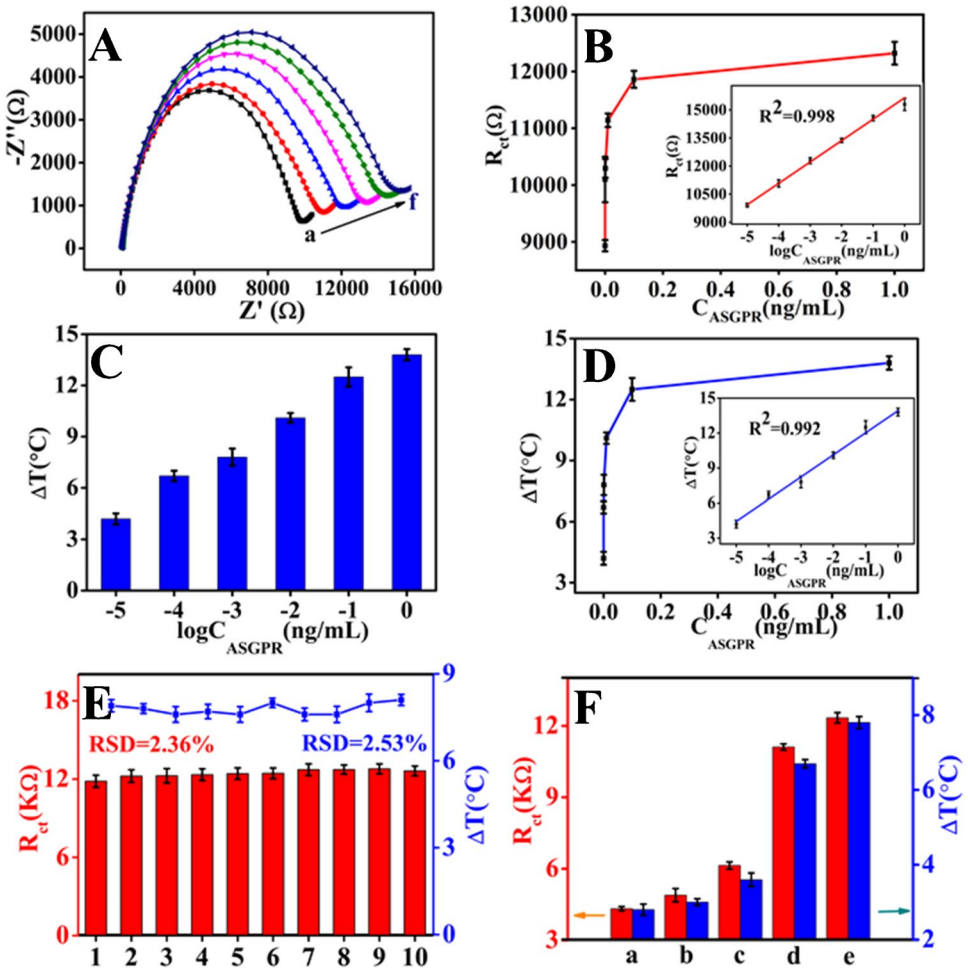

Fig. 5 **A** The EIS responses and **B** calibration curve of the immunosensor for the detection of different concentrations of ASGPR (a–f: 10^{-5}, 10^{-4}, 10^{-3}, 10^{-2}, 10^{-1}, and 1 ng/mL) with laser irradiation for 30 s; **C** temperature histograms for ASGPR detection of different concentrations 10^{-5}–1 ng/mL (left to right); **D** the corresponding linear relationship between temperature and the concentration of target ASGPR. **E** The stability of the immunosensor by EIS detection (curve red) and photothermal detection (curve blue). **F** The specificity of the immunosensor toward different interferences of 0.01 ng/mL (a) E6, (b) LSR, (c) IL-6, (d) mix, and (e) $10.^{-3}$ ng/mL ASGPR by EIS detection (curve red) and photothermal detection (curve blue)

The regression fitting equation was $R_{ct} = 1143.0 \lg C + 15{,}651$ ($R^2 = 0.998$), and the limit of detection (LOD) was as low as 3.3×10^{-6} ng/mL. Therefore, through the change of impedance, the concentration of ASGPR could be well detected. At the same time, the temperature changes caused by different concentrations of ASGPR under laser irradiation (808 nm, 2.5 w/cm^2) were also recorded. As shown in Fig. 5C, the increase in temperature was proportional to the logarithm of the ASGPR concentration. In addition, the regression equation was $\Delta T = 1.8960 \lg C + 13.921$ ($R^2 = 0.992$), the linear range was 10^{-5} to 1 ng/mL, and the LOD was 3.3×10^{-6} ng/mL (Fig. 5D). Another type of immunosensor was also prepared and compared without PNIPAM modification (sensor A) with the developed immunosensor (sensor B) (Figure S4). Compared with other reported ASGPR detection methods (Table S3), the constructed EIS immunosensor had a wider linear range and high sensitivity; therefore, the developed immunosensor was more sensitive and convincing.

In order to further explore the analytical performance of the immunosensor, ten sets of parallel experiments were performed by incubating 10^{-3} ng/mL ASGPR on the electrode to verify the repeatability of the immunosensor. As shown in Fig. 5E, the relative standard deviation (RSD) of the EIS response was 2.36%. In addition, the RSD of temperature was 2.53%, indicating that the immunosensor had good stability.

Selectivity played an important role in evaluating immunosensing. Figure 5F shows that by adding 0.01 ng/mL E6, LSR, IL-6, mix, and 10^{-3} ng/mL ASGPR, its EIS signal and temperature change. As expected, the EIS and temperature response of the target ASGPR and the mixture increased significantly. However, interferences had little effect on the detection results. Due to specific immune recognition, the dual-readout scheme had good selectivity for ASGPR.

Real sample analysis

This study used the standard addition method to explore the practical application value of the dual-readout immunosensor. The human serum sample was diluted 100 times with pH 7.4 PBS, and then, three different concentrations of ASGPR standard solutions were added to the diluted sample serum (Table S2), the recoveries ranged from 96.1 to 108%, suggesting that the dual-readout immunosensor could be used for ASGPR detection in serum samples.

Conclusion

A dual-readout immunosensor based on a multifunctional MXene probe triggered signal amplification was constructed for the detection of ASGPR. Temperature-sensitive PNIPAM was used as sensing substrates, which could be used to adjust the conductivity of electrode interfaces. Importantly, under 808-nm laser irradiation, Nb_2C MXene acted as a photothermal converter to increase the local temperature of the electrode surface, causing the PNIPAM to undergo a shrinkage phase transition, thereby achieving photothermal-triggered EIS signal amplification. This work opened up a new way for the combination of electrochemical impedance and other detection methods, and provided a sensitive detection method for the diagnosis of hepatitis A disease.

Supplementary Information The online version contains supplementary material available at https://doi.org/10.1007/s00604-022-05350-1.

Funding We gratefully acknowledge the financial supports from the National Natural Science Foundation of China (21877012, 21575024), the National Science Foundation of Fujian Province (2020J02034, 2019J01052063), and the Health-Education Joint Research Project of Fujian Province (2019-WJ-04).

Declarations

Conflict of interest The authors declare no competing interests.

References

1. Sun P, Zhu Y, Han Y, Hu K, Huang S, Wang M, Wu H, Tang G (2020) Radiosynthesis and biological evaluation of an fluorine-18 labeled galactose derivative F-18 FPGal for imaging the hepatic asialoglycoprotein receptor, Bioorg Med Chem Lett 30(12)
2. Pintó RM, Pérez-Rodríguez F-J, Costafreda M-I, Chavarria-Miró G, Guix S, Ribes E, Bosch A (2021) Pathogenicity and virulence of hepatitis A virus, Taylor & Francis - 12(- 1) - 1185
3. Friedman SL (2000) Molecular regulation of hepatic fibrosis, an integrated cellular response to tissue injury. J Biol Chem 275(4):2247–2250
4. Havelaar AH, Kirk MD, Torgerson PR, Gibb HJ, Hald T, Lake RJ, Praet N, Bellinger DC, De Silva NR, Gargouri N, Speybroeck N, Cawthorne A, Mathers C, Stein C, Angulo FJ, Devleesschauwer B (2015) World Hlth Org Foodborne Dis, World Health Organization Global Estimates and Regional Comparisons of the Burden of Foodborne Disease in 2010, Plos Medicine 12(12)
5. Li K-B, Li N, Zang Y, Chen G-R, Li J, James TD, He X-P, Tian H (2016) Foldable glycoprobes capable of fluorogenic crosslinking of biomacromolecules. Chem Sci 7(10):6325–6329
6. Shen D, Liu J, Sheng L, Lv Y, Wu G, Wang P, Du K (2020) Design, synthesis and evaluation of a novel fluorescent probe to accurately detect H2S in hepatocytes and natural waters, Spectrochim Acta Part a-Mol Biomol Spectrosc 228
7. Qu B, Zhang X, Wang Z, Liu Y, Zhang H, Zhang R (2019) A novel magnetic resonance contrast agent for detection of hepatic segmental function. Mater Lett 254:452–456
8. Li G, Zhu M, Ma L, Yan J, Lu X, Shen Y, Wan Y (2016) Generation of small single domain nanobody binders for sensitive detection of testosterone by electrochemical impedance spectroscopy. ACS Appl Mater Interfaces 8(22):13830–13839
9. Akter R, Jeong B, Lee Y-M, Choi J-S, Rahman MA (2017) Femtomolar detection of cardiac troponin I using a novel label-free and reagent-free dendrimer enhanced impedimetric immunosensor. Biosens Bioelectron 91:637–643
10. Wang J, Zhang S, Dai H, Zheng H, Hong Z, Lin Y (2019) Dual-readout immunosensor constructed based on brilliant photoelectrochemical and photothermal effect of polymer dots for sensitive detection of sialic acid, Biosens Bioelectron 142
11. Chen Y, Zhang S, Hong Z, Lin Y, Dai H (2019) A mimotope peptide-based dual-signal readout competitive enzyme-linked immunoassay for non-toxic detection of zearalenone. J Mater Chem B 7(44):6972–6980
12. Chen Y, Jiang B, Xiang Y, Chai Y, Yuan R (2011) Target recycling amplification for sensitive and label-free impedimetric genosensing based on hairpin DNA and graphene/Au nanocomposites. Chem Commun 47(48):12798–12800
13. Ren H, Han Q, Zhang S, Huang Y, Chen Y, Dai H, Yan J, Lin Y (2020) A photothermal assisted in situ signal-amplified electrochemical immunoassay based on multifunctional probe for detecting autoimmune hepatitis marker, Sensors and Actuators B-Chemical 309
14. Contento NM, Semancik S (2016) Thermal characteristics of temperature-controlled electrochemical microdevices. Sensors and Actuators B-Chemical 225:279–287
15. Huang L, Chen J, Yu Z, Tang D (2020) Self-powered temperature sensor with Seebeck effect transduction for photothermal-thermoelectric coupled immunoassay. Anal Chem 92(3):2809–2814
16. Khazaei M, Arai M, Sasaki T, Chung C-Y, Venkataramanan NS, Estili M, Sakka Y, Kawazoe Y (2013) Novel electronic and magnetic properties of two-dimensional transition metal carbides and nitrides. Adv Func Mater 23(17):2185–2192
17. Lin H, Gao S, Dai C, Chen Y, Shi J (2017) A two-dimensional biodegradable niobium carbide (MXene) for photothermal tumor eradication in NIR-I and NIR-II biowindows. J Am Chem Soc 139(45):16235–16247
18. Fu G, Sanjay ST, Zhou W, Brekken RA, Kirken RA, Li X (2018) Exploration of nanoparticle-mediated photothermal effect of TMB-H2O2 colorimetric system and its application in a visual quantitative photothermal immunoassay. Anal Chem 90(9):5930–5937
19. Lin H, Wang X, Yu L, Chen Y, Shi J (2017) Two-dimensional ultrathin MXene ceramic nanosheets for photothermal conversion. Nano Lett 17(1):384–391
20. Lee SH, Choi S, Kwon K, Bae N-H, Kwak BS, Cho WC, Lee SJ, Junga H-I (2017) A photothermal biosensor for detection of C-reactive protein in human saliva. Sensors and Actuators B-Chemical 246:471–476
21. Xia N, Huang Y, Cui Z, Liu S, Deng D, Liu L, Wang J (2020) Impedimetric biosensor for assay of caspase-3 activity and evaluation of cell apoptosis using self-assembled biotin-phenylalanine network as signal enhancer, Sensors and Actuators B-Chemical 320
22. Xue S, Li Q, Wang L, You W, Zhang J, Che R (2019) Copper- and cobalt-codoped CeO2 nanospheres with abundant oxygen vacancies as highly efficient electrocatalysts for dual-mode electrochemical sensing of microRNA. Anal Chem 91(4):2659–2666
23. Hou L, Zhang X, Kong M, Jiang G, Sun Y, Mo W, Lin T, Ye F, Zhao S (2020) A competitive immunoassay for electrochemical impedimetric determination of chlorpyrifos using a nanogold-modified glassy carbon electrode based on enzymatic biocatalytic precipitation, Microchimica Acta 187(4)
24. Litowczenko J, Gapinski J, Markiewicz R, Wozniak A, Wychowaniec JK, Peplinska B, Jurga S, Patkowski A (2021) Synthesis, characterization and in vitro cytotoxicity studies of poly-N-isopropyl acrylamide gel nanoparticles and films, Mater Sci Eng C-Mater Biol Appl 118

25. Liu R, Cao W, Han D, Mo Y, Zeng H, Yang H, Li W (2019) Nitrogen-doped Nb2CTx MXene as anode materials for lithium ion batteries. J Alloy Compd 793:505–511
26. Mutharani B, Ranganathan P, Chen S-M, Vishnu DSK (2020) Stimuli-enabled reversible switched aclonifen electrochemical sensor based on smart PNIPAM/PANI-Cu hybrid conducting microgel, Sensors Actuators B-Chem 304
27. Yang T, Fu J, Zheng S, Yao H, Jin Y, Lu Y, Liu H (2018) Biomolecular logic devices based on stimuli-responsive PNIPAM-DNA film electrodes and bioelectrocatalysis of natural DNA with Ru(bpy)(3)(2+) as mediator. Biosens Bioelectron 108:62–68
28. Jastrzebska A, Szuplewska A, Rozmyslowska-Wojciechowska A, Mitrzak J, Wojciechowski T, Chudy M, Moszczynska D, Wojcik A, Prenger K, Naguib M (2020) Juggling surface charges of 2D niobium carbide MXenes for a reactive oxygen species scavenging and effective targeting of the malignant melanoma cell cycle into programmed cell death. Acs Sustain Che Eng 8(21):7942–7951
29. Arif N, Gul S, Sohail M, Rizwan S, Iqbal M (2021) Synthesis and characterization of layered Nb2C MXene/ZnS nanocomposites for highly selective electrochemical sensing of dopamine. Ceram Int 47(2):2388–2396
30. Yang J, Liao M, Hong G, Dai S, Shen J, Xie H, Chen C (2020) Effect of APTES- or MPTS-conditioned nanozirconia fillers on mechanical properties of Bis-GMA-based resin composites. ACS Omega 5(50):32540–32550
31. Hua M, Wu D, Wu S, Ma Y, Alsaid Y, He X (2021) 4D printable tough and thermoresponsive hydrogels. ACS Appl Mater Interfaces 13(11):12689–12697